Control Engineering Practice 85 (2019) 280–289

Contents lists available at ScienceDirect

Control Engineering Practice

journal homepage: www.elsevier.com/locate/conengprac

State and unknown input estimation of an anaerobic digestion reactor with experimental validation

L. Dewasme [a,*], M. Sbarciog [a], E. Rocha-Cózatl [b], F. Haugen [c], A. Vande Wouwer [a]

[a] Automatic Control Laboratory, University of Mons, 31, Boulevard Dolez, 7000 Mons, Belgium
[b] Departamento de Ingeniería Mecatrónica, Universidad Nacional Autónoma de México, 4510, Mexico, D.F., Mexico
[c] University of South-Eastern Norway, Norway

ARTICLE INFO

Keywords:
Kalman filter
Robust estimation
Sensitivity analysis
Software sensors
Bioprocesses

ABSTRACT

This paper investigates state and unknown input estimations in an Anaerobic Digestion Reactor (ADR) considering a simple two-stage reaction model describing acidogenesis and methanogenesis. From the sole methane outlet flow, this model allows to predict the inlet and outlet biodegradable suspended solid and volatile fatty acid concentrations, which are critical for process stability, as well as acidogenic and methanogenic biomasses. Continuous–discrete exogenous and unknown input formulations of the Extended Kalman Filter (EKF) are applied in this context and a numerical robustness analysis is achieved to characterize sensitivities to measurement noise and model uncertainties. The resulting observers are then validated experimentally with data from a lab-scale plant.

1. Introduction

Anaerobic digestion (AD) is a complex biological process driven by several bacteria populations, which can be roughly classified in acidogenic biomass, consuming biodegradable matter and producing volatile fatty acids (VFA), and methanogenic biomass, consuming VFA and producing biogas (a mixture of mostly carbon dioxide and methane). This process is increasingly implemented in the field of solid and liquid waste treatment and represents an important source of renewable energy, which can also be combined to other process units in biorefineries. AD processes present complex dynamics, are sensitive to input fluctuations, and are generally delicate to start and operate in the presence of perturbations. Process control is therefore required, which in turn, imposes the availability of on-line measurements of key-components such as VFA concentrations. In practice, however, measurement information is quite limited and it is necessary to resort to software sensors, which blend the information of a process model and of some available online probes.

The problem of AD process state estimation has attracted attention, and several alternative approaches have been proposed. For instance, Alcaraz-Gonzalez and Gonzalez-Alvarez (2007) suggests the use of an asymptotic observer allowing the reconstruction of the process state despite the lack of knowledge of the kinetics. Unfortunately, this kind of observers is quite sensitive to unknown process inputs. An improved version called "virtually controlled observer" (VCO), which compensates the observation error by adjusting the input information has recently been developed by the same authors (Alcaraz-Gonzalez, Jauregui-Medina, Steyer, Garcìa-Sandoval, Méndez-Acosta, & Gonzalez-Alvarez, 2017). As a counterpart, the VCO requires on-line measurements of VFA and total inorganic carbon (TIC). Another robust estimation approach is based on interval estimation. A bundle of interval observers can be built to estimate an envelope of the state trajectory (i.e., state lower and upper bounds) (Alcaraz-Gonzalez & Gonzalez-Alvarez, 2007; Moisan & Bernard, 0000). The main advantage of this approach is that it is possible to take account of uncertainties in the model parameters, initial conditions and inputs in a flexible way. On the other hand, the estimated intervals can be conservative and delicate to exploit if a tight control is required. Other recent proposals include an experimentally-validated fuzzy observer (Carlos-Hernandez, Sanchez, & Béteau, 2009), a Luenberger-type observer (Didi, Dibb, & Cherkia, 2015) and a robust observer with sigmoid-type output injection (Lara-Cisneros, Aguilar-López, Dochain, & Femat, 2016). However, these latter works do not consider the issue of unknown input concentrations and the impact that these perturbations can have on state estimation.

This particular issue is addressed in the present work, which focuses attention on the design of unknown input observers (UIO) for monitoring the AD process. UIO are dynamical systems that robustly estimate the state variables with respect to the disturbances or unknown inputs that affect the system. For example, the authors have

* Corresponding author.
E-mail addresses: Laurent.Dewasme@umons.ac.be (L. Dewasme), Mihaela@Sbarciog.be (M. Sbarciog), e.rocha.cozatl@comunidad.unam.mx (E. Rocha-Cózatl), finn.haugen@usn.no (F. Haugen), Alain.VandeWouwer@umons.ac.be (A.V. Wouwer).

https://doi.org/10.1016/j.conengprac.2019.02.003
Received 24 August 2018; Received in revised form 10 December 2018; Accepted 9 February 2019
Available online xxxx

proposed in Sbarciog, Moreno, and Vande Wouwer (2014) the design of an UIO consisting of three parts, i.e., two super twisting observers (i.e., second-order sliding mode observers) and an asymptotic observer for estimating two biomass concentrations and two inlet substrate concentrations in an AD process described by a two-step reaction model. The proposed sliding mode UIO is efficient but requires the on-line measurements of the organic substrate and volatile fatty acid concentrations, which is a practical limitation. The current study alleviates this limitation and takes a more practical approach based on the sole measurement of the methane flow rate (biogas flow rate and biogas composition are nowadays standard measurements in many anaerobic digesters). To efficiently handle measurement noise, minimum variance (Kalman-like) filters are exploited, in continuation to the preliminary work reported in Rocha-Cózatl, Sbarciog, Dewasme, Moreno, and Vande Wouwer (2015). In the same spirit as Haugen, Bakke, and Lie (2013, 2014), which applies an unscented Kalman filter, an Extended Kalman Filter (EKF), complemented by an exogenous system for the partial description of the unknown input (i.e., based on some assumptions such as slow-varying perturbations) is first designed. Alternatively, an UIO filter developed by Gillijns and De Moor (2007), and extended to nonlinear continuous-time models associated to discrete-time (and often rare) measurements in Rocha-Cózatl, Moreno, and Vande Wouwer (2012), is considered. The Exogenous-Input Extended Kalman Filter (EIEKF) and the Unknown-Input Extended Kalman Filter (UIEKF) are compared in the situation where only the outlet methane flow rate is available as on-line measurement. Furthermore, the approach is validated with experimental data from a pilot plant (whereas our previous study (Sbarciog et al., 2014) was limited to simulation, because of the difficulty to achieve the more extensive measurement configuration required by this proposal).

This paper is organized as follows. The next section presents the AD process model. An observability analysis is provided in Section 3 in accordance with the available measurements. Section 4 reviews the two estimation methods and Section 5 presents a robustness analysis of the observers, setting their parameters in accordance with specific disturbance/input profile cases and compares their performances. Experimental validations of the EIEKF and UIEKF are assessed in Section 6 while conclusions are drawn in Section 7.

2. A simple two-step model

Several two-step reaction models have been proposed in the last decades, including Bernard, Hadj-Sadok, Dochain, Genovesi, and Steyer (2001), Beteau, Otton, Hihn, Delpech, and Chéruy (2005), Escudié, Conte, Steyer, and Delgenès (2005), Hill (1983) and Rozzi (1984). Some of these models aim at accurately describing the kinetic as well as the hydrodynamic characteristics of the process. From a control point of view, it is necessary to find a good compromise between model complexity and prediction accuracy. In this context, Donoso-Bravo, Mailier, Martin, Rodriguez, Aceves-Lara, and Vande Wouwer (2011) reviews most of the existing anaerobic digestion models and discusses various model properties and parameter identification issues.

Among the above-mentioned models, the model proposed by Hill (1983) is adopted in the present study. It consists of four mass balance ordinary differential equations:

$$\dot{S}_{bvs} = \left(S_{bvs_{in}} - S_{bvs}\right)\frac{F_{feed}}{V} - \mu\left(S_{bvs}\right)k_1 X_{acid} \tag{1a}$$

$$\dot{S}_{vfa} = \left(S_{vfa_{in}} - S_{vfa}\right)\frac{F_{feed}}{V} + \mu\left(S_{bvs}\right)k_2 X_{acid} - \mu_c\left(S_{vfa}\right)k_3 X_{meth} \tag{1b}$$

$$\dot{X}_{acid} = \left(\mu\left(S_{bvs}\right) - K_d - \frac{F_{feed}/b}{V}\right)X_{acid} \tag{1c}$$

$$\dot{X}_{meth} = \left(\mu_c\left(S_{vfa}\right) - K_{dc} - \frac{F_{feed}/b}{V}\right)X_{meth} \tag{1d}$$

Table 1
Identified parameter values of Hill's model (Hill, 1983).

$A_f = 0.69$	$[(gVFA/L)/(gBVS/L)]$
$B_0 = 0.25$	$[(gBVS/L)/(gVS/L)]$
$b = 2.90$	$[d/d]$
$k_1 = 3.89$	$[gBVS/(g\ acidogens/L)]$
$k_2 = 1.76$	$[gVFA/(g\ acidogens/L)]$
$k_3 = 31.7$	$[gVFA/(g\ methanogens/L)]$
$k_5 = 26.3$	$[L/g\ methanogens]$
$K_d = 0.02$	$[d^{-1}]$
$K_{dc} = 0.02$	$[d^{-1}]$
$K_s = 15.5$	$[gBVS/L]$
$K_{sc} = 3$	$[gVFA/L]$
$V = 250$	$[L]$
$T_{reac} = 35$	[°C]

where S_{bvs} is the concentration of organic substrate (biodegradable volatile solids) in $[gBVS/L]$, S_{vfa} is the concentration of volatile fatty acids in $[gVFA/L]$, X_{acid} represents the acidogenic bacteria in $[g\ acidogens/L]$, and X_{meth} the methanogenic bacteria in $[g\ methanogens/L]$. The factor $\frac{F_{feed}}{V}$ represents the dilution rate in $[(LCH_4/d)/L]$, and k_1, k_2, k_3 are the stoichiometric coefficients.

It is considered that the inlet biodegradable volatile solid and volatile fatty acid concentrations are fractions of the total inlet raw waste concentration $S_{vs_{in}}$ as in:

$$S_{bvs_{in}} = B_0 S_{vs_{in}} \tag{2a}$$

$$S_{vfa_{in}} = A_f S_{bvs_{in}} = A_f B_0 S_{vs_{in}} \tag{2b}$$

The first equation therefore defines the fraction of raw waste which can serve as substrate for the acidogenic biomass (biodegradable part) while the second equation defines the fraction of that biodegradable material which is initially in the acid form. Parameters B_0 and A_f are considered as in the original Hill model (Hill, 1983) and can be obtained from laboratory tests. In this way, both inlet concentrations depend on $S_{vs_{in}}$, which is considered as an unknown input.

The measurable output is the methane gas flow rate (gas production) in $[LCH_4/d]$ given by

$$F_{meth} = V\mu_c\left(S_{vfa}\right)k_5 X_{meth} \tag{3}$$

The reaction rate kinetic functions are modeled by Monod laws:

$$\mu\left(S_{bvs}\right) = \mu_m \frac{S_{bvs}}{K_s + S_{bvs}} \tag{4a}$$

$$\mu_c\left(S_{vfa}\right) = \mu_{mc} \frac{S_{vfa}}{K_{sc} + S_{vfa}} \tag{4b}$$

where the maximum reaction rates μ_m and μ_{mc} are functions of the reactor temperature

$$\mu_m\left(T_{reac}\right) = \mu_{mc}\left(T_{reac}\right) = 0.013T_{reac} - 0.129 \tag{5}$$

for 20 [°C] $< T_{reac} <$ 60 [°C], and K_s and K_{sc} are the half-saturation constants.

The considered values of the model parameters are summarized in Table 1.

3. Observability analysis

Hill's model (1) is a nonlinear dynamic system of the form

$$\dot{\xi} = f\left(\xi, u, w\right) \tag{6a}$$

$$y = h\left(\xi\right) \tag{6b}$$

where the state vector $\xi = \left[S_{bvs}, S_{vfa}, X_{acid}, X_{meth}\right]$, the known input $u = D = \frac{F_{feed}}{V}$, the unknown input $w = S_{vs_{in}}$, and the measured output $y = F_{meth}$.

System observability relates to the possibility of estimating the system state based on the available measurement information, i.e., in spite of the lack of information about the true initial conditions.

Definition. A general nonlinear system is observable if

$$\forall t_0, \exists t_1 < \infty | y\left(t; t_0, \xi(0), u(t)\right) = y\left(t; t_0, \xi'(0), u(t)\right), \quad \forall u(t), t_0 < t < t_1 \Rightarrow \xi(0) = \xi'(0). \tag{7}$$

A system is observable if two identical output trajectories y (function of time t, the initial states $\xi(0)$ and of the input $u(t)$) over a given finite time horizon imply the equality of the initial states $\xi(0)$ and $\xi'(0)$. Observability analysis of nonlinear systems is not a trivial task. Several approaches have been proposed, including the concept of canonical observability forms (Gauthier & Kupka, 1994; Zeitz, 1984) or inference diagrams (Liu, Slotine, & Barabási, 2013) for large and complex systems. However, when some inputs are unknown, the analysis becomes even more difficult and Moreno, Rocha-Cózatl, and Vande Wouwer (2013) suggests a method based on the analysis of the error dynamics. This method is now briefly introduced and applied to Hill's model.

From (1) and (2) – using the notation of (6a) – the following state–space representation of the system is obtained:

$$\dot{\xi}_1 = (B_0 w - \xi_1)u - \mu(\xi_1)k_1\xi_3 \tag{8a}$$

$$\dot{\xi}_2 = (A_f B_0 w - \xi_2)u + \mu(\xi_1)k_2\xi_3 - \mu_c(\xi_2)k_3\xi_4 \tag{8b}$$

$$\dot{\xi}_3 = (\mu(\xi_1) - K_d - \frac{u}{b})\xi_3 \tag{8c}$$

$$\dot{\xi}_4 = (\mu_c(\xi_2) - K_{dc} - \frac{u}{b})\xi_4 \tag{8d}$$

with

$$\mu = \mu_m \frac{\xi_1}{\xi_1 + K_S} \tag{9a}$$

$$\mu_c = \mu_{mc} \frac{\xi_2}{\xi_2 + K_{Sc}} \tag{9b}$$

A copy of the system is built, where the state vector is denoted $x = [x_1, x_2, x_3, x_4]$, the unknown input $\bar{w}$ and the measured output y_x, respectively.

$$\dot{x}_1 = (B_0 \bar{w} - x_1)u - \mu(x_1)k_1 x_3 \tag{10a}$$

$$\dot{x}_2 = (A_f B_0 \bar{w} - x_2)u + \mu(x_1)k_2 x_3 - \mu_c(x_2)k_3 x_4 \tag{10b}$$

$$\dot{x}_3 = (\mu(x_1) - K_d - \frac{u}{b})x_3 \tag{10c}$$

$$\dot{x}_4 = (\mu_c(x_2) - K_{dc} - \frac{u}{b})x_4 \tag{10d}$$

with

$$\mu = \mu_m \frac{x_1}{x_1 + K_S} \tag{11a}$$

$$\mu_c = \mu_{mc} \frac{x_2}{x_2 + K_{Sc}} \tag{11b}$$

The deviation between the original system (8), (9) and its copy (10) and (11) is described by the error system:

$$\dot{\epsilon}_1 = B_0 u (w - \bar{w}) - u\epsilon_1 - \mu_m k_1 \phi_1\left(x_1, x_3, \epsilon_1, \epsilon_3\right) \tag{12a}$$

$$\dot{\epsilon}_2 = A_f B_0 u (w - \bar{w}) - u\epsilon_2 + \mu_m k_2 \phi_1\left(x_1, x_3, \epsilon_1, \epsilon_3\right) - \mu_{mc} k_3 \phi_2\left(x_2, x_4, \epsilon_2, \epsilon_4\right) \tag{12b}$$

$$\dot{\epsilon}_3 = -\left(K_d + \frac{u}{b}\right)\epsilon_3 + \mu_m \phi_1\left(x_1, x_3, \epsilon_1, \epsilon_3\right) \tag{12c}$$

$$\dot{\epsilon}_4 = -\left(K_{dc} + \frac{u}{b}\right)\epsilon_4 + \mu_{mc} \phi_2\left(x_2, x_4, \epsilon_2, \epsilon_4\right) \tag{12d}$$

where the error variable $\epsilon = \xi - x$, and the functions:

$$\phi_1\left(x_1, x_3, \epsilon_1, \epsilon_3\right) = \frac{\left(x_1 + \epsilon_1\right)\left(x_3 + \epsilon_3\right)}{K_s + \left(x_1 + \epsilon_1\right)} - \frac{x_1 x_3}{K_s + x_1} \tag{13a}$$

$$\phi_2\left(x_2, x_4, \epsilon_2, \epsilon_4\right) = \frac{\left(x_2 + \epsilon_2\right)\left(x_4 + \epsilon_4\right)}{K_{sc} + \left(x_2 + \epsilon_2\right)} - \frac{x_2 x_4}{K_{sc} + x_2} \tag{13b}$$

The output error $e = y - y_x$ is given by

$$e = V k_5 \mu_{mc} \phi_2\left(x_2, x_4, \epsilon_2, \epsilon_4\right) \tag{14}$$

If, for each known pair u, y (which implies $e = 0$, i.e. $y = y_x$), the only solution is $\epsilon = 0$, then there is distinguishability of the states and the system is observable. Detectability corresponds to an asymptotic decay $\epsilon \to 0$. In addition, if the analysis implies $w = \bar{w}$, then there is distinguishability of the inputs, and the unknown input can be estimated.

In the case of Hill's model, $e = 0$ implies that $\phi_2(\cdot) = 0$, and in turn that $\dot{\epsilon}_4 = -\left(K_{dc} + \frac{u}{b}\right)\epsilon_4$. This latter equation implies that $\epsilon_4 \to 0$ since both K_{dc} and u/b are positive values. From the definition of $\phi_2(\cdot)$ one can prove that if $\epsilon_4 \to 0$ then $\epsilon_2 \to 0$.

To proceed further with the analysis, one can define $\epsilon_A = \epsilon_2 - A_f \epsilon_1$, and write the remaining system as

$$\dot{\epsilon}_A = -u\epsilon_A + \left(\mu_m k_2 + \mu_m k_1 A_f\right)\phi_1\left(x_1, x_3, \epsilon_A, \epsilon_3\right) \tag{15a}$$

$$\dot{\epsilon}_3 = -\left(K_d + \frac{u}{b}\right)\epsilon_3 + \mu_m \phi_1\left(x_1, x_3, \epsilon_A, \epsilon_3\right) \tag{15b}$$

An analytic solution seems difficult at this stage, and we resort to numerical simulation coupled to an equilibrium stability analysis (see in Appendix) to study the system dynamics and the convergence of the error to the origin. In Fig. 1, a Monte Carlo study is achieved by varying the error initial condition $\epsilon(0)$ (for the sake of clarity, the values are normalized with respect to the true initial condition). 200 runs are generated, which correspond to the simulation of the process over a period of 300 days with constant input. 6 different Gaussian distributions of the error, with standard deviations σ_e of 10, 20, 30, 40, 50 and 60%, are considered (so, on the whole, 1200 runs are generated). No diverging trajectory (with respect to $(0, 0)$) appears below $\sigma_e = 50\%$, for which 3 diverging runs are observed out of 200. The situation slightly worsens for $\sigma_e = 60\%$, with 6 diverging runs. Each of these runs actually reaches a physical boundary imposed to ϵ_3, i.e., $x_3 = 0$ or $\epsilon_3 = -\xi_3$, which represents the acidogenic biomass wash-out. It is obvious that, in this particular case, the system becomes unobservable.

These results show that the (not washed-out) system is globally observable as long as the stability condition (38) developed in Appendix is respected. From Eq. (12a), detectability of the states induces detectability of the unknown input since $\epsilon_1 \to 0$ implies, for a non-zero input, that $w = \bar{w}$.

4. State and input estimation

In bioprocess applications, states can generally be measured at discrete times only and with relatively low sampling frequencies (the measurements are sometimes collected at different rates, i.e., resulting in an asynchronous measurement configuration). A continuous–discrete observer formulation, where continuous estimation is provided from discrete-time measurements, is therefore appropriate. Consider the nonlinear continuous-time model with discrete-time measurements (16a)–(16b)

$$\dot{\xi} = f(\xi, u, w) + \omega \tag{16a}$$

$$y_{[k]} = h\left(\xi_{[k]}\right) + \nu_{[k]} \tag{16b}$$

where $\xi \in \mathbb{R}^n$ is the state vector, $u \in \mathbb{R}^r$ is the manipulated (known) input vector, $w \in \mathbb{R}^p$ is the vector of unknown perturbations, and $\omega \in \mathbb{R}^n$ is the vector of system noise. $y \in \mathbb{R}^m$ is the output (measurement) vector. We assume that ω and $\nu_{[k]}$ are stationary zero-mean white noise processes with covariance matrices Q and R. In addition, we assume that ξ_0, ω and $\nu_{[k]}$ are uncorrelated.

In the spirit of the extended Kalman filter, the nonlinear model (16a) can be linearized along the state trajectory

$$\delta\dot{\xi} = A(t)\delta\xi + B(t)\delta u + B_w(t)\delta w, \tag{17a}$$

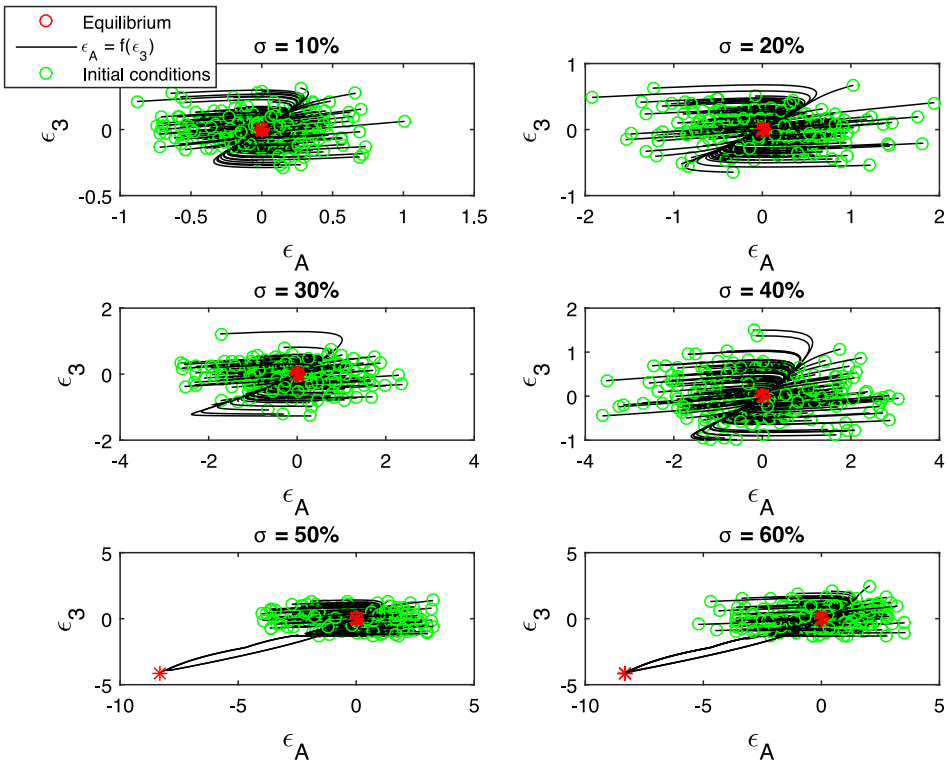

Fig. 1. Monte Carlo study: error system trajectories (black lines) initiated from various initial errors (green circles). The resulting errors (after 300 days) are represented by red stars . (For interpretation of the references to color in this figure legend, the reader is referred to the web version of this article.)

$$\delta y_{[k]} = C(t)\,\delta\xi_{[k]} \tag{17b}$$

where $A(t) = \frac{\partial f}{\partial \xi}\left(\xi(t), u_{[k|k]}, w_{[k|k]}\right)$, $B(t) = \frac{\partial f}{\partial u}\left(\xi(t), u_{[k|k]}, w_{[k|k]}\right)$, $B_w(t) = \frac{\partial f}{\partial w}\left(\xi(t), u_{[k|k]}, w_{[k|k]}\right)$ and $C(t) = \frac{\partial h}{\partial \xi}(\xi(t))$. This model can also be expressed in a full discrete-time form as

$$\delta\xi_{[k+1]} = A_{[k]}\delta\xi_{[k]} + B_{[k]}\delta u_{[k]} + B_{w[k]}\delta w_{[k]}, \tag{18a}$$

$$\delta y_{[k]} = C(t)\,\delta\xi_{[k]} \tag{18b}$$

4.1. Extended Kalman filter and definition of an exogenous input

The traditional formulation of the continuous–discrete Extended Kalman Filter (EKF) (Simon, 2006) is the following

- Measurement Update

$$\hat{\xi}_{[k|k]} = \hat{\xi}_{[k|k-1]} + L_{[k]}\left(y_{[k]} - h\left(\hat{\xi}_{[k|k-1]}\right)\right) \tag{19a}$$

$$L_{[k]} = P_{[k|k-1]}C^T\mathcal{R} \tag{19b}$$

$$P_{[k|k]} = P_{[k|k-1]} - P_{[k|k-1]}C^T\mathcal{R}CP_{[k|k-1]} \tag{19c}$$

  where $\mathcal{R} = \left(CP_{[k|k-1]}C^T + R\right)^{-1}$ and P is the covariance matrix of the estimation error.
- Time Update

$$\dot{\hat{\xi}} = f\left(\hat{\xi}, u, w\right) \tag{20a}$$

$$\dot{P} = A(t)P + PA^T(t) + Q \tag{20b}$$

$$\hat{\xi}_{[k+1|k]} = \hat{\xi}((k+1)T) \tag{21a}$$

$$P_{[k+1|k]} = P((k+1)T) \tag{21b}$$

When it is not possible to measure the input w, an exogenous system can be defined, based on some plausible assumption. A new state variable $\xi_{n+1} = w$ can be introduced based on the assumption of slow variations (i.e., a sufficiently fast sampling) according to $\dot{\xi}_{n+1} = \omega_{n+1}$, where ω_{n+1} is a zero-mean white noise signal (which is equivalent to a random walk).

4.2. Continuous–discrete unknown input observer

A more sophisticated alternative is provided by the UIO formulation of Gillijns and De Moor (2007), which is extended to nonlinear systems in Rocha-Cózatl et al. (2012). Following the model linearization, a linear state–space representation in the form of (18) (i.e., in variation around a point or trajectory) is obtained. The continuous–discrete UIEKF allows the estimation of δw, as in Gillijns and De Moor (2007). The prediction step is achieved using the original nonlinear model, starting from the last corrected state and, since w is unknown on the prediction interval, the last estimated value of this input. The propagation of the covariance matrix P is the same as in the standard EKF.

The continuous–discrete UIEKF is given by the following equations:

- Estimation of the Unknown Input

$$\bar{R}_{[k]} = C\bar{P}_{[k|k-1]}C^T + R \tag{22a}$$

$$\bar{\mathcal{M}}_{[k]} = \left(F_{[k]}^T\bar{R}_{[k]}^{-1}F_{[k]}\right)^{-1}F_{[k]}^T\bar{R}_{[k]}^{-1} \tag{22b}$$

$$\delta\hat{w}_{[k-1|k]} = \bar{\mathcal{M}}_{[k]}\left(y_{[k]} - h\left(\hat{\bar{x}}_{[k|k-1]}\right)\right) \tag{22c}$$

$$\hat{w}_{[k-1|k]} = \hat{w}_{[k-1|k-1]} + \delta\hat{w}_{[k-1|k]} \tag{22d}$$

$$P_{w[k|k]} = \left(F_{[k]}^T\bar{R}_{[k]}^{-1}F_{[k]}\right)^{-1} \tag{22e}$$

  where $F_{[k]} = CB_{w[k]}$.
- Measurement update

$$\hat{\bar{\xi}}_{[k|k]} = \hat{\bar{\xi}}_{[k|k-1]} + B_{w[k-1]}\delta\hat{w}_{[k-1|k]} \tag{23a}$$

$$\bar{L}_{[k]} = \bar{P}_{[k|k-1]}C^T\bar{R}_{[k]}^{-1} \tag{23b}$$

$$\bar{P}_{[k|k]} = \bar{P}_{[k|k-1]} + B_{w[k-1]}P_{w[k-1|k]}B_{w[k-1]}^T - B_{w[k-1]}P_{w[k-1|k]}F_{[k-1]}^T\bar{L}_{[k]}^T \tag{23c}$$

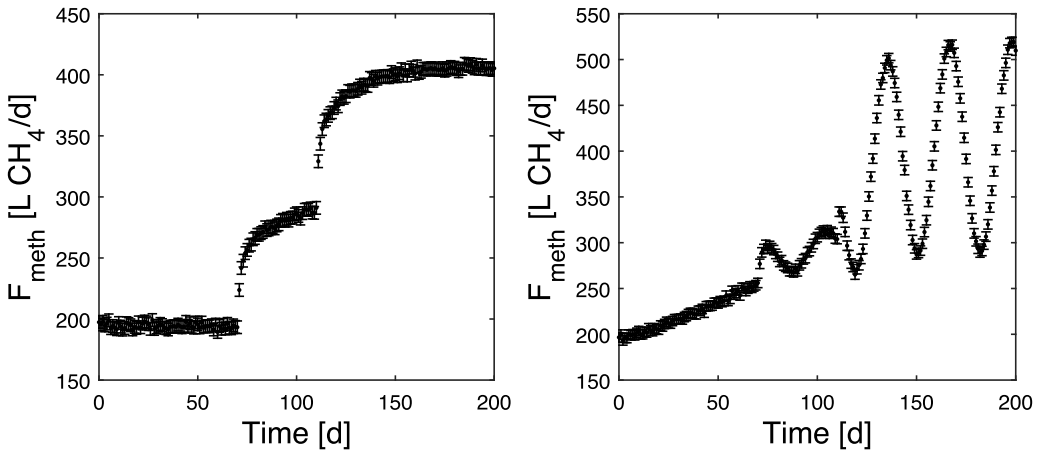

Fig. 2. Output measurements represented by error bars with a 99% confidence related to measurement error standard deviation $\sigma_{meas} = 2\ [LCH_4/d]$.

$$- \bar{L}_{[k]} F_{[k-1]} P_{w[k-1|k]} B^T_{w[k-1]}$$

$$\hat{\xi}_{[k|k]} = \hat{\bar{\xi}}_{[k|k]} + \bar{L}_{[k]} \left(y_{[k]} - h\left(\hat{\bar{\xi}}_{[k|k]} \right) \right) \tag{23d}$$

$$P_{[k|k]} = \bar{P}_{[k|k]} - \bar{L}_{[k]} \left(\bar{R}_{[k]} - F_{[k-1]} P_{w[k-1|k]} F^T_{[k-1]} \right) \bar{L}^T_{[k]} \tag{23e}$$

- Time Update

$$\dot{\hat{\xi}} = f\left(\hat{\xi}, u_{[k]}, w_{[k-1|k]} \right) \tag{24a}$$

$$\dot{P} = A(t) P + P A^T(t) + Q \tag{24b}$$

with $A(t) = \frac{\partial f}{\partial \xi}\left(\hat{\xi}(t), u_{[k|k]} \right)$.

$$\hat{\bar{\xi}}_{[k+1|k]} = \hat{\xi}((k+1)T) \tag{25a}$$

$$P_{[k+1|k]} = P((k+1)T) \tag{25b}$$

An estimate of the unknown input $w_{[k-1|k]}$ can be obtained with one sampling time delay (as the measurement in k contains information on the unknown input in $k-1$, as reflected in (22c)).

5. Robustness analysis of estimation strategies: simulation results

This section is dedicated to a simulation study where the relative performance of EIEKF and UIEKF is assessed. The nonlinear model (1) is considered with the numerical values of the parameters reported in Table 1 (Haugen et al., 2013). The parameters are perturbed in order to investigate the robustness of the estimation strategy.

In this context, the output $y = F_{meth}$ (methane flow rate) is assumed to be measured once a day ($T = 1d$) with a measurement error characterized by a standard deviation $\sigma_{meas} = 2\ [LCH_4/d]$. This value is larger than the one used in Haugen et al. (2013, 2014), where $\sigma_{meas} = 1.2[LCH_4/d]$.

The process initial conditions are defined as $S_{bvs}(0) = B_0\ 30$, $S_{vfa}(0) = B_0\ A_f\ 30$, $X_{acid}(0) = 0.2\ [gX_{acid}/L]$, $X_{meth}(0) = 0.2\ [gX_{meth}/L]$, whereas the observer initial conditions are randomly distributed following a Gaussian law centered in the process initial conditions with a relative standard deviation defined as $\epsilon_{IC} = 20\%$ (the detectability analysis presented in Section 3 does not indicate that specific limits should be imposed to the initial error, but 20% seems a realistic standard deviation).

The known input feed flow rate $F_{feed} = 55\ L/d$ is constant.

5.1. Observer design

The observer design involves the selection of covariance matrices P_0, R and Q, which will be the same for both observers. To test the observer performance, two distinct case studies are considered: (1) the unknown input follows a step-wise evolution (in agreement with the exogenous model of the EIEKF) and parametric errors with 10% relative standard deviation are considered; (2) the unknown input has additional dynamics (signal made of ramps and sinusoids) while the parametric errors are smaller (limited to 2% of relative standard deviation).

The covariance matrices and operating conditions are therefore defined as follows:

- The initial covariance of the estimation errors P_0 is defined as a diagonal matrix with elements $P_{0_{i,i}} = \left[\epsilon_{IC} x_i(0)\right]^2$.
- The covariance of the measurement errors R is a scalar, since there is a single measurement output $y = F_{meth}$, i.e., $R = 4\ [LCH_4/d]^2$.
- In case study 1, the unknown input concentration $S_{vs_{in}}$ is defined as a step-wise function:

$$S_{vs_{in}}(t) = \begin{cases} 30 \quad [gVS/L] & 0 \le t \le 70 \\ 40 \quad [gVS/L] & 70 < t \le 110 \\ 50 \quad [gVS/L] & 110 < t \le 200 \end{cases} \tag{26}$$

whereas in case study 2, the unknown input evolves successively as a ramp, a low-magnitude sinusoid and a high-magnitude sinusoid:

$$S_{vs_{in}}(t) = \begin{cases} 30 + 0.1\ t & [gVS/L] & 0 \le t \le 70 \\ 40 + 3\ sin(0.2\ t) & [gVS/L] & 70 < t \le 110 \\ 50 + 15\ sin(0.2\ t) & [gVS/L] & 110 < t \le 200 \end{cases} \tag{27}$$

The output measurements corresponding to these two cases are shown in Fig. 2.

- The covariance of the process errors Q is considered as a diagonal matrix, whose elements are selected either as $Q_{i,i} = \left[0.1\hat{x}_i(0)\right]^2$ in case study 1 or $Q_{i,i} = \left[0.04\hat{x}_i(0)\right]^2$ in case study 2. The tuning of the matrix Q is achieved in an ad-hoc manner, so as to compensate for larger parametric uncertainties in case 1 (in both cases, the process noise level is related to the magnitude of the state).

Note that in the case of the EIEKF, the initial estimated state vector is augmented by the unknown input as:

$$\hat{x}_i(0) = \left[\hat{S}_{bvs}(0), \hat{S}_{vfa}(0), \hat{X}_{acid}(0), \hat{X}_{meth}(0), \hat{S}_{vs_{in}}(0) \right] \tag{28}$$

5.2. Numerical simulation results

Model and observer ordinary differential equations (ODEs) (16a), (20) and (24) are solved using the Matlab solver *ode15s*, which is a stiff ODE solver. This alleviates potential issues related to the stability of numerical integration and the reduction of the time stepsize to

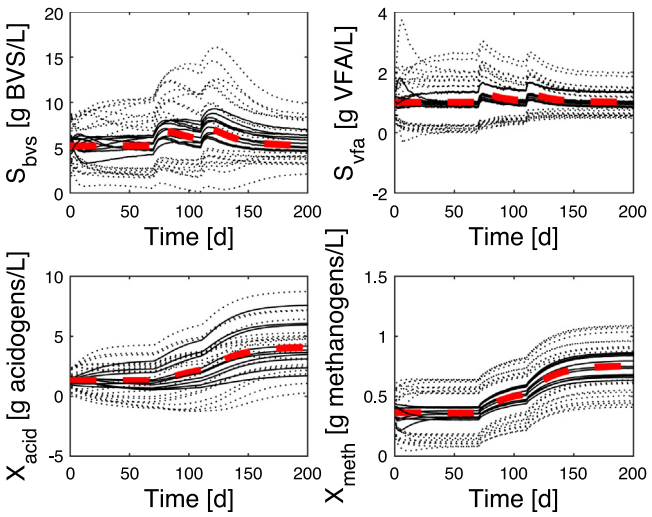

Fig. 3. Time evolution of the state variables in case 1. Red dashed lines: process state trajectories; black solid lines: EIEKF estimates (for 10 different perturbations in the parameter set); dotted lines: bounds of the estimation confidence intervals.

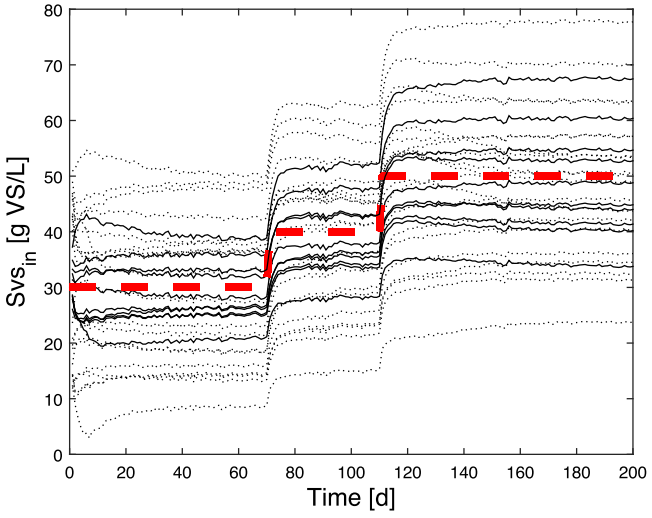

Fig. 4. Unknown input estimation in case 1. Red dashed lines: input evolution; black solid lines: EIEKF estimates (for 10 different perturbations in the parameter set); dotted lines: bounds of the 99% confidence intervals.

accommodate different time scales. Figs. 3 and 4 show the results of 10 simulation runs of EIEKF in case 1, where the whole model parameter set of the predictor is subject to random variations centered in the nominal values with a relative standard deviation of 10%. The same study is achieved for the UIEKF and the results are shown in Figs. 5 and 6.

The performance of both observers is quite satisfactory. 99% confidence intervals can be drawn (dotted lines in the several figures) using the information provided by matrices P (of dimensions 5×5 for the EIEKF and 4×4 for the UIEKF) and P_u (only for the UIEKF) showing the reliability of the estimates.

In order to quantify the estimation of the unknown input, the root mean square (RMSE) and the standard deviation of the estimation error $e = S_{VSin} - \hat{S}_{VSin}$, are listed in Table 2, which also shows the results of 10 Monte Carlo analyses (corresponding to 10 sets of perturbed parameters), each of them comprising 50 runs (corresponding to 50 sets of initial conditions).

The average behavior (RMSE) of the unknown input estimation error is quite similar for both observers but its spread (standard deviation) is significantly different, with an advantage to the EIEKF with

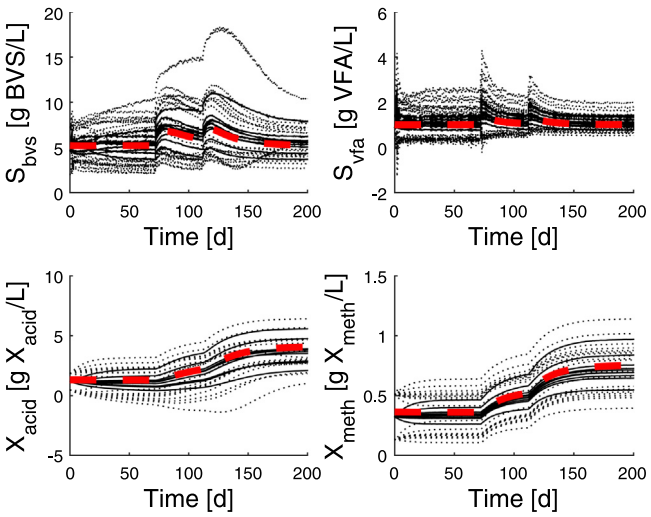

Fig. 5. Time evolution of the state variables in case 1. Red dashed lines: process state trajectories; black solid lines: UIEKF estimates (for 10 different perturbations in the parameter set); dotted lines: bounds of the 99% confidence intervals.

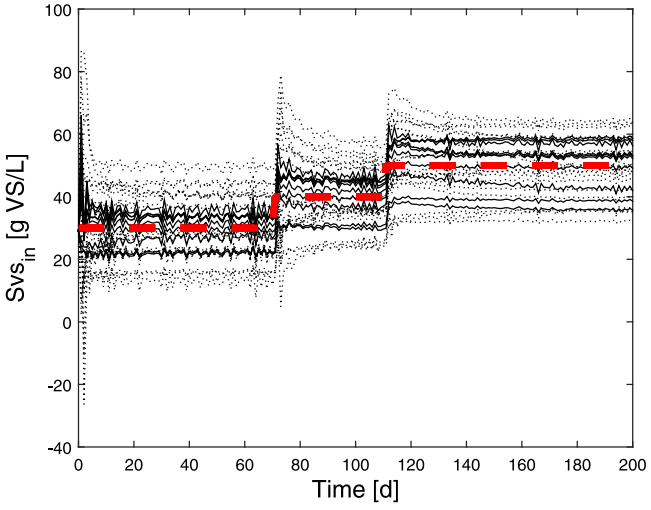

Fig. 6. Unknown input estimation in case 1. Red dashed lines: input evolution; black solid lines: UIEKF estimates (for 10 different perturbations in the parameter set); dotted lines: bounds of the 99% confidence intervals.

Table 2
Characterization of the unknown input estimation error of EIEKF and UIEKF (results of a Monte Carlo analysis).

	EIEKF	UIEKF
RMSE (gVS/L)	5.68	5.81
Standard deviation (gVS/L)	1.63	2.58

that respect. The UIEKF is obviously more sensitive to the measurement noise.

To deepen the analysis, case 2 is now illustrated in Figs. 7 and 8. Clearly, the UIEKF offers a better convergence rate than the EIEKF, whose exogenous model now does fit well the signal shape. Again, the estimates of the UIEKF are noisier reflecting the higher sensitivity to measurement errors.

6. Experimental validation

The reactor is a UASBR (Upflow Anaerobic Sludge Blanket Reactor) and is part of the Foss Biolab, a pilot plant for nutrient and energy

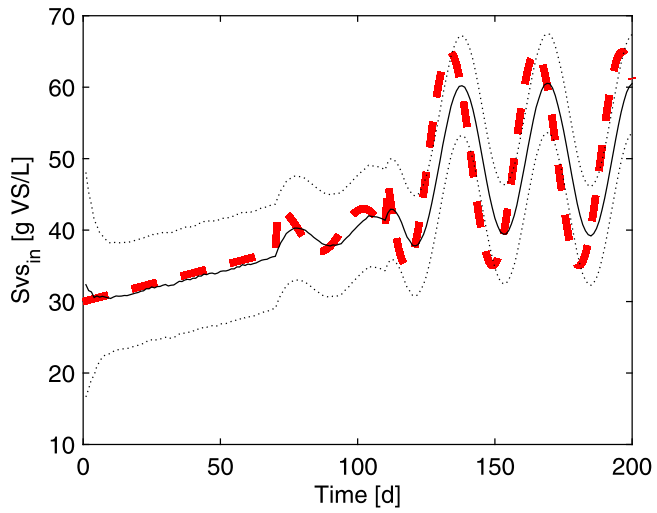

Fig. 7. Unknown input estimation in case 2. Red dashed line: input trajectory; black solid line: EIEKF estimated input; dotted lines: bounds of the 99% confidence intervals.

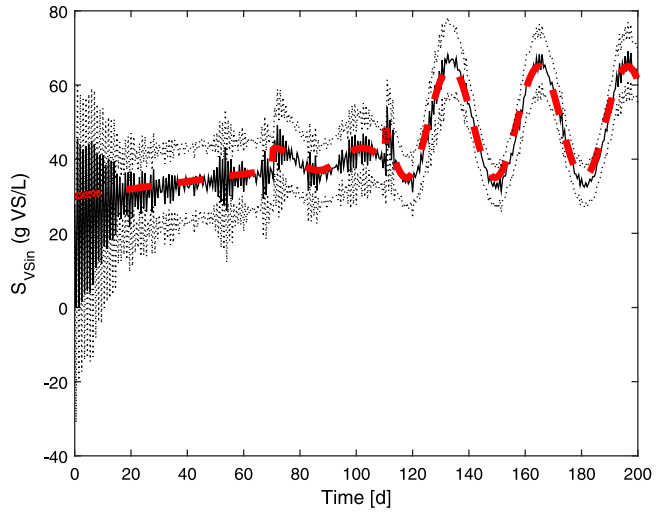

Fig. 8. Unknown input estimation in case 2. Red dashed line: input trajectory; black solid line: UIEKF estimated input; dotted lines: bounds of the 99% confidence intervals.

recovery situated at Foss Farm, Skien. The operating conditions are detailed in Haugen et al. (2013, 2014), and the temperature and feed flow are shown in Fig. 9. The feed flow F_{feed} varies between 30 and 70 L/d which is of the same order of magnitude as the feed flow F_{feed} = 45 L/d considered in the numerical simulation results of Section 5.2. The temperature T is almost constant and was set accordingly to 35 °C in the simulation studies.

Table 3
Characterization of EIEKF and UIEKF estimation errors during the experimental validation.

	EIEKF	UIEKF
Input RMSE (gVS/L)	2.1	2.07
S_{bvs} RMSE (gBVS/L)	0.56	0.69
S_{vfa} RMSE (gVFA/L)	0.38	0.38
Input standard deviation (gVS/L)	1.6	1.73
S_{bvs} standard deviation (gBVS/L)	0.46	0.64
S_{vfa} standard deviation (gVFA/L)	0.22	0.27

Although the experiment was conducted over more than 320 days, attention is focused on the period ranging from $t = 85\ d$ to $t = 320\ d$.

To assess the observer performance, the data relative to the substrates S_{bvs} and S_{vfa}, input $S_{vs_{in}}$ and output F_{meth} is considered in the sequel. Note that the analytic equipment did not allow to collect information about the acidogenic and methanogenic bacterial populations.

The observer estimates are shown in Figs. 10–13. They are quite good from the beginning until $t = 170h$, when S_{vfa} is slightly overestimated as well as the input S_{VSin}. At the same time, temperature undergoes a sudden variation of 0.2 °C, which could be one of the factors explaining the observed deviation. Biomass estimates cannot be compared to experimental values and are checked for consistency.

Quantitative observations made in Section 5.2 are still valid as shown in Table 3. The RMSEs are quite similar whereas UIEKF is more sensitive to measurement errors.

7. Conclusions

Anaerobic digestion is a complex biological process requiring advanced monitoring techniques for process optimization and control. A large body of published reports is available regarding state estimation in AD. However, most of these studies assume that (i) different key-components are measurable on line (increasing investment costs), (ii) the model can be reduced to a single reaction (decreasing the interpretability of the results), (iii) the inlet concentrations are constant or can be measured on-line (which is either restrictive or again implies additional investments for reactor instrumentation). This study therefore proposes practical solutions to the problem of state and unknown input estimation for ADR. These solutions are based on a simple two-stage reaction model, which allows to predict the evolution of the volatile fatty acids, as well as the acidogenic and methanogenic bac-

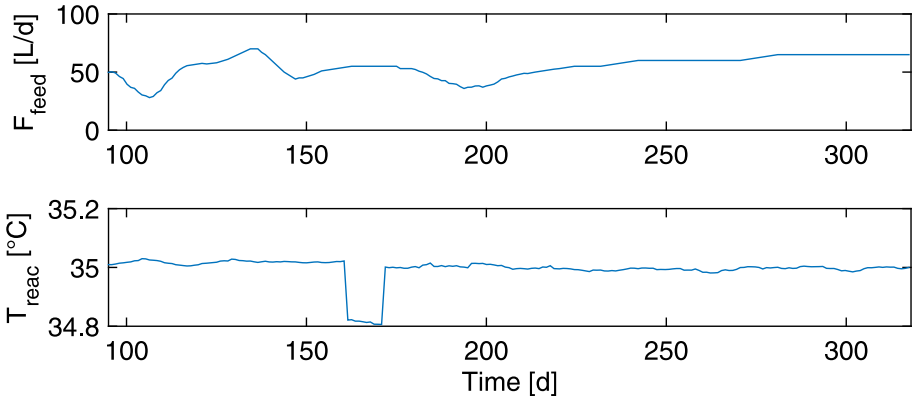

Fig. 9. Experimental operating conditions: evolutions of the inlet flow and temperature.

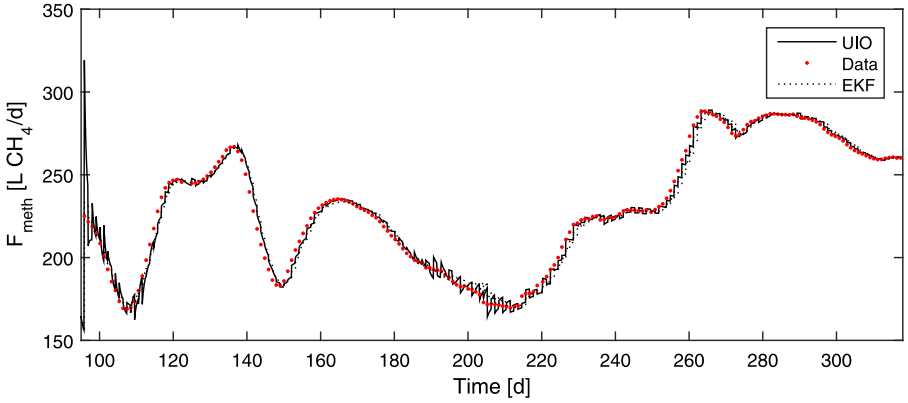

Fig. 10. Output flow estimates provided by EIEKF and UIEKF — experimental validation. Red dots: experimental data; black dotted line: EIEKF; black Solid line: UIEKF.

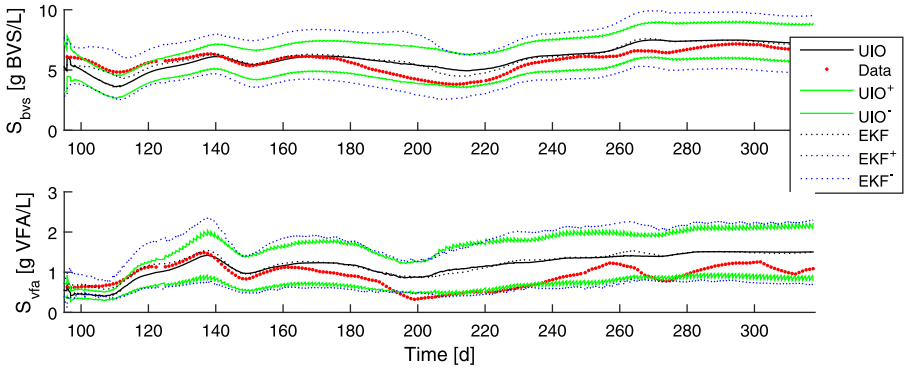

Fig. 11. Substrate estimates provided by EIEKF and UIEKF — experimental validation. Red dots: experimental data; black dotted line: EIEKF; blue dotted lines: EIEKF confidence intervals at 99%; black solid line: UIEKF; green solid lines: UIEKF confidence intervals at 99% . (For interpretation of the references to color in this figure legend, the reader is referred to the web version of this article.)

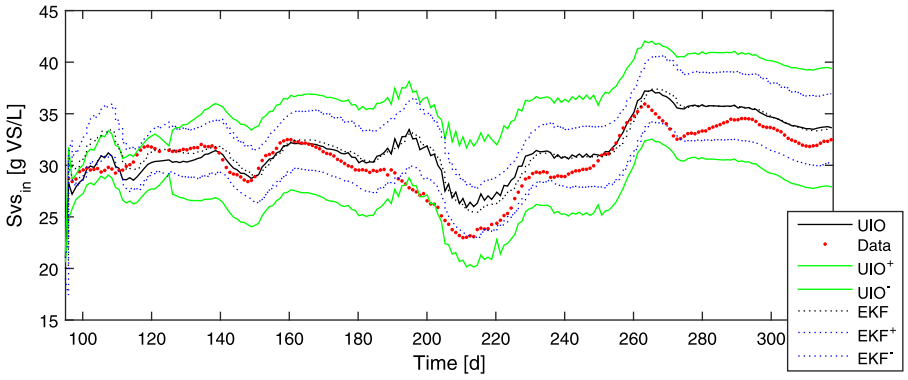

Fig. 12. Input estimates provided by EIEKF and UIEKF — experimental validation. Red dots: experimental data; black dotted line: EIEKF; blue dotted lines: EIEKF confidence intervals at 99%; black solid line: UIEKF; green solid lines: UIEKF confidence intervals at 99% . (For interpretation of the references to color in this figure legend, the reader is referred to the web version of this article.)

terial populations. Continuous–discrete exogenous input and unknown input formulations of the Extended Kalman Filter can be developed on this basis, providing quite satisfactory results, as demonstrated through both numerical robustness analysis and experimental validation. Generally, the unknown input extended Kalman filter provides fast convergence in a wide range of conditions, but is more sensitive to measurement noise than the exogenous input extended Kalman filter, which is slightly less versatile due to the need of defining the type of unknown signals affecting the reactor.

Acknowledgments

The authors gratefully acknowledge the support of FNRS, Belgium and CONACYT, Mexico in the framework of a joint research project, which made possible several research stays in Mons and Mexico City.

Conflict of interest

Conflict of interest - None declared

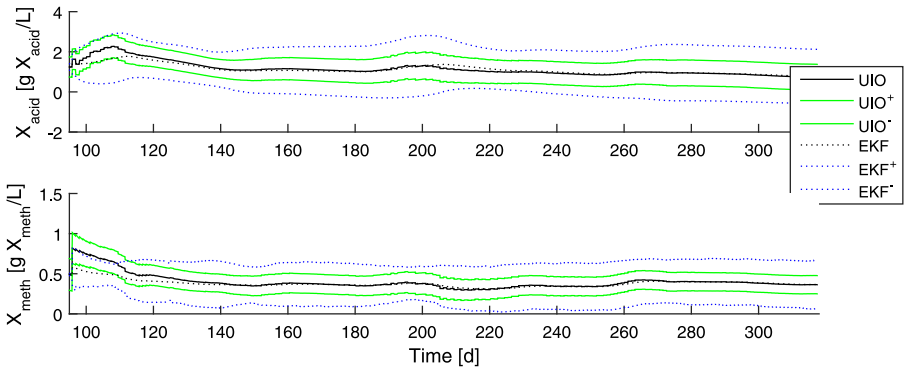

Fig. 13. Biomass estimates provided by EIEKF and UIEKF — experimental validation. Black dotted line: EIEKF; blue dotted lines: EIEKF confidence intervals at 99%; black solid line: UIEKF; green solid lines: UIEKF confidence intervals at 99% . (For interpretation of the references to color in this figure legend, the reader is referred to the web version of this article.)

Appendix. Study of the equilibria of the error system

The equilibrium points of the error system (15) are calculated from:

$$-\left(K_d+\frac{u}{b}\right)\epsilon_3+\mu_m\phi_1=0 \tag{29a}$$

$$-\epsilon_A u+\left(k_2+A_f k_1\right)\phi_1=0 \tag{29b}$$

where, for simplicity, $\phi_1(.)$ is replaced with ϕ_1. From (29b), $\phi_1=\frac{(K_d+u/b)}{\mu_m}\epsilon_3$, which in combination with (29a), provides:

$$\epsilon_A=A(u)\epsilon_3 \tag{30}$$

with $A(u)=\left(k_2+A_f k_1\right)\frac{\left(K_d+\frac{u}{b}\right)}{u}$.

Eq. (30) establishes the global mapping defining the equilibria with respect to the input u.

Using the expression of ϕ_1 given by (13a) in (29b), where $\epsilon_1=-\epsilon_A/A_f$, and performing some trivial mathematical manipulations, one may find that:

$$\epsilon_A\left\{u\left[\left(K_s+x_1\right)^2-\frac{\epsilon_A}{A_f}\left(K_s+x_1\right)\right]\right.$$
$$\left.-\mu_m\left(k_2+A_f k_1\right)\left[\frac{x_1}{A}\left(K_s+x_1\right)-x_3\frac{K_s}{A_f}-\frac{\epsilon_A}{A_f A}\left(K_s+x_1\right)\right]\right\}=0 \tag{31}$$

The two solutions of (31) can be written as:

$$\epsilon_{A1}=0 \tag{32a}$$

$$\epsilon_{A2}=\frac{A_f\left(K_d+\frac{u}{b}\right)}{u\left[\mu_m-\left(K_d+\frac{u}{b}\right)\right]}\left[\mu_m\frac{ux_1}{K_d+\frac{u}{b}}-\mu_m\left(k_2+A_f k_1\right)\frac{x_3K_s}{A_f\left(K_s+x_1\right)}-u\left(K_s+x_1\right)\right] \tag{32b}$$

The local stability of the reduced error system (15) may be studied by computing the eigenvalues at the two equilibria. To this end, the system Jacobian matrix is computed as:

$$J\left(\epsilon_A,\epsilon_3\right)=\begin{bmatrix}\frac{\partial f_1(\epsilon_A,\epsilon_3)}{\partial\epsilon_A} & \frac{\partial f_1(\epsilon_A,\epsilon_3)}{\partial\epsilon_3}\\ \frac{\partial f_3(\epsilon_A,\epsilon_3)}{\partial\epsilon_A} & \frac{\partial f_3(\epsilon_A,\epsilon_3)}{\partial\epsilon_3}\end{bmatrix} \tag{33}$$

where $f_1(\epsilon_A,\epsilon_3)$ and $f_3(\epsilon_A,\epsilon_3)$, respectively, denote the right hand sides of Eqs. (15). The components of (33) are calculated as

$$\frac{\partial f_1(\epsilon_A,\epsilon_3)}{\partial\epsilon_A}=-u+\mu_m\left(k_2+A_f k_1\right)\frac{\partial\phi_1}{\partial\epsilon_A} \tag{34a}$$

$$\frac{\partial f_1(\epsilon_A,\epsilon_3)}{\partial\epsilon_3}=\mu_m\left(k_2+A_f k_1\right)\frac{\partial\phi_1}{\partial\epsilon_3} \tag{34b}$$

$$\frac{\partial f_3(\epsilon_A,\epsilon_3)}{\partial\epsilon_A}=\mu_m\frac{\partial\phi_1}{\partial\epsilon_A} \tag{34c}$$

$$\frac{\partial f_3(\epsilon_A,\epsilon_3)}{\partial\epsilon_3}=-\left(K_d+\frac{u}{b}\right)+\mu_m\frac{\partial\phi_1}{\partial\epsilon_3} \tag{34d}$$

The eigenvalues are the solutions of the equation $det\left|J\left(\epsilon_A,\epsilon_3\right)-\lambda I_2\right|=0$, where $det|.|$ denotes the determinant and I_2 is the identity matrix of dimension two. Taking into account that ϵ_A and ϵ_3 are related by (30), one can rewrite ϕ_1 as a function ϵ_3 only. As a consequence, $\frac{\partial\phi_1}{\partial\epsilon_A}=0$. Hence, the characteristic equation becomes

$$(-u-\lambda)\left(-\left(K_d+u/b\right)+\mu_m\frac{\partial\phi_1}{\partial\epsilon_3}-\lambda\right)=0 \tag{35}$$

and the eigenvalues are

$$\lambda_1=-u \tag{36a}$$

$$\lambda_2=-\left(K_d+u/b\right)+\mu_m\frac{\partial\phi_1}{\partial\epsilon_3} \tag{36b}$$

Note that $\lambda_1<0$ as $u>0$ and the stability of the two equilibria is entirely determined by the sign of λ_2.

Computing

$$\frac{\partial\phi_1}{\partial\epsilon_3}=\frac{\frac{-A}{A_f}K_s\left(x_3+\epsilon_3\right)+\left(x_1-\frac{A}{A_f}\epsilon_3\right)\left(K_s+x_1-\frac{A}{A_f}\epsilon_3\right)}{\left(K_s+x_1-\frac{A}{A_f}\epsilon_3\right)^2} \tag{37}$$

it may be concluded that the equilibrium point $(\epsilon_A,\epsilon_3)=(0,0)$ is stable if

$$\mu_m\frac{x_1}{K_s+x_1}<\left(K_d+\frac{u}{b}\right)+\mu_m\frac{A(u)}{A_f}\frac{K_sx_3}{\left(K_s+x_1\right)^2} \tag{38}$$

Fig. 14 shows the evolution of the right hand side of (38), named f_2, with respect to x_1 and x_3 for different values of the input u chosen in a realistic range according to the experimental conditions of Fig. 9. The intersection of f_2 with f_2^*, the left hand side of (38), is represented in red, defining a boundary between the stable and unstable zones. Globally, the $(\epsilon_A=0,\epsilon_3=0)$ equilibrium may be reached as long as, for a defined inlet flow level, acidogenic biomass and biodegradable volatile solid concentrations are not evolving too close to wash-out and overflow, respectively (and at the same time).

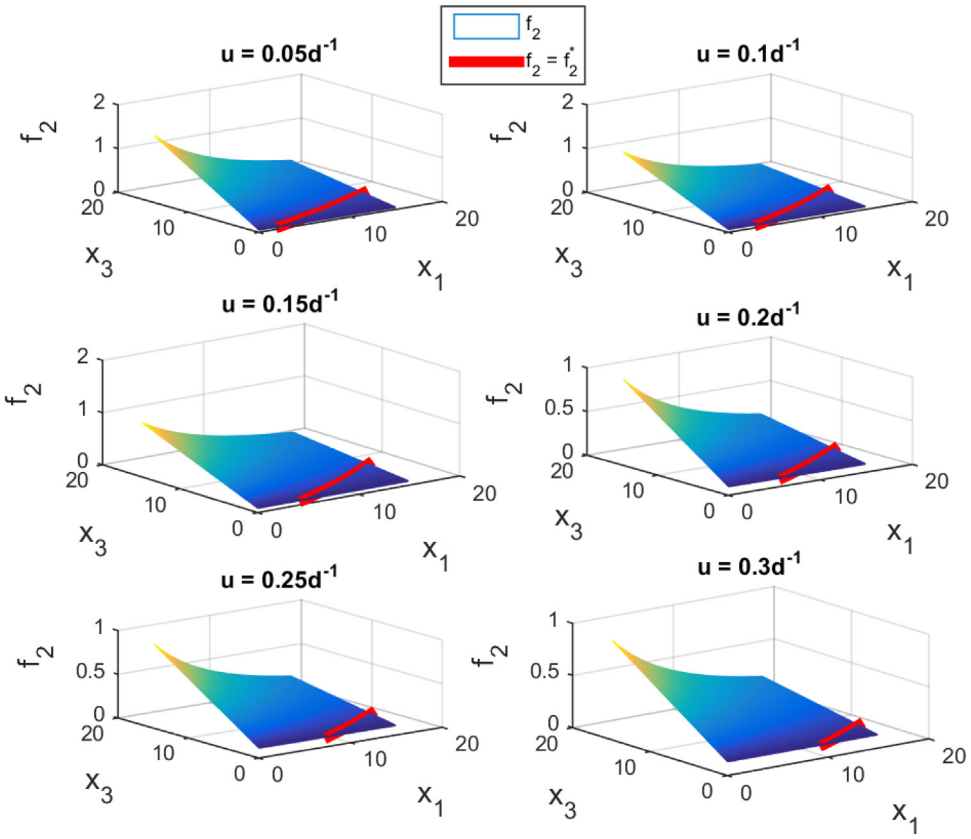

Fig. 14. Stability diagram: evolution of $f_2 = \left(K_d + \frac{u}{b}\right) + \mu_m \frac{A(u)}{A_f} \frac{K_s x_3}{(K_s + x_1)^2}$ with respect to x_1 and x_3 for different u (input) values in a realistic operating range. Intersection of f_2 with $f_2^* = \mu_m \frac{x_1}{K_s + x_1}$ is represented by the red boundary . (For interpretation of the references to color in this figure legend, the reader is referred to the web version of this article.)

References

Alcaraz-Gonzalez, V., & Gonzalez-Alvarez, V. (2007). Robust nonlinear observers for bioprocesses: Application to wastewater treatment. In H. O. Mendez-Acosta, R. Femat, & V. Gonzalez-Alvarez (Eds.), *Springer LNCIS 361, Dynamics and Control of Chemical and Bioplogical Processes* (pp. 119–164).

Alcaraz-Gonzalez, V., Jauregui-Medina, E. A., Steyer, J. Ph., Garcìa-Sandoval, J. P., Méndez-Acosta, H. O., & Gonzalez-Alvarez, V. (2017). Simultaneous COD and VFA unmeasured process inputs estimation in actual anaerobic wastewater treatment processes. *Control Engineering Practice*, *60*, 118–123.

Bernard, O., Hadj-Sadok, Z., Dochain, D., Genovesi, A., & Steyer, J.-P. (2001). Dynamical model development and parameter identification for anaerobic wastewater treatment process. *Biotechnology and Bioengineering*, *75*, 424–438.

Beteau, J.-F., Otton, V., Hihn, J.-Y., Delpech, F., & Chéruy, A. (2005). Modelling of anaerobic digestion in a fluidised bed with a view to control. *Biochemical Engineering Journal*, *24*, 255–267.

Carlos-Hernandez, S., Sanchez, E. N., & Béteau, J. F. (2009). Fuzzy observers for anaerobic WWTP:development and implementation. *Control Engineering Practice*, *17*, 690–702.

Didi, I., Dibb, H., & Cherkia, B. (2015). A Luenberger-type observer for the AM2 model. *Journal of Process Control*, *32*, 117–126.

Donoso-Bravo, A., Mailier, J., Martin, C., Rodriguez, J., Aceves-Lara, C. A., & Vande Wouwer, A. (2011). Model selection, identification and validation in anaerobic digestion: A review. *Water Research*, *45*, 5347–5364.

Escudié, R., Conte, T., Steyer, J.-P., & Delgenès, J.-P. (2005). Hydrodynamic and biokinetic models of an anaerobic fixed-bed reactor. *Process Biochemistry*, *40*, 2311–2323.

Gauthier, J.-P., & Kupka, I. (1994). Observability and observers for nonlinear systems. *SIAM Journal Control and Optimization*, *32*(4), 975–994.

Gillijns, S., & De Moor, B. (2007). Unbiased minimum-variance input and state estimation for linear discrete-time systems. *Automatica*, *43*, 111–116.

Haugen, F., Bakke, R., & Lie, B. (2013). Adapting dynamic mathematical models to a pilot anaerobic digestion reactor. *Modeling. Identification & Control*, [ISSN: 1890-1328] *34N*(2), 35–54.

Haugen, F., Bakke, R., & Lie, B. (2014). State Estimation and Model-Based Control of a Pilot Anaerobic Digestion Reactor. Journal of Control Science and Engineering. Hindawi Publishing Corporation. Volume 2014, Article ID 572621, 19 pages. http://dx.doi.org/10.1155/2014/572621.

Hill, D. T. (1983). Simplified monod kinetics of methane fermentation of animal wastes. *Agricultural Wastes*, *5*, 1–16.

Lara-Cisneros, G., Aguilar-López, R., Dochain, D., & Femat, R. (2016). On-line estimation of VFA concentration in anaerobic digestion via methane outflow rate measurements. *Computers & Chemical Engineering*, *94*, 250–256.

Liu, Y.-Y., Slotine, J.-J., & Barabási, A.-L. (2013). Observability of complex systems. *Proceedings of the National Academy of Sciences of the United States of America*, *110*(7), 2460–2465.

Moisan, M., & Bernard, O. An interval observer for non-monotone systems: application to an industrial anaerobic digestion process. In *10th International IFAC symposium on computer applications in biotechnology, vol. 1* (pp. 325-330).

Moreno, J. A., Rocha-Cózatl, E., & Vande Wouwer, A. (2013). A dynamical interpretation of strong observability and detectability concepts for nonlinear systems with unknown inputs: application to biochemical processes. *Bioprocess and Biosystems Engineering*, http://dx.doi.org/10.1007/s00449-013-0915-5, Published online in www.springer.com.

Rocha-Cózatl, E., Moreno, J. A., & Vande Wouwer, A. (2012). Application of a continuous-discrete unknown input observer to estimation in phytoplanktonic cultures. In *Preprints of the 8th IFAC symposium on advanced control of chemical processes (ADCHEM) 2012, Singapore*.

Rocha-Cózatl, E., Sbarciog, M., Dewasme, L., Moreno, J. A., & Vande Wouwer, A. (2015). State and input estimation of an anaerobic digestion reactor using a continuous-discrete unknown input observer. *IFAC-PapersOnLine*, *48*(8), 129–134, Preprints of the 9th IFAC Symposium on Advanced Control of Chemical Processes (ADCHEM) 2015, Whistler, Canada.

Rozzi, A. (1984). Modelling and control of anaerobic digestion process. *Transactions of Institute of Measurement & Control*, *6*(3), 153–159.

Sbarciog, M., Moreno, J. A., & Vande Wouwer, A. (2014). Application of super-twisting observers to the estimation of state and unknown inputs in an anaerobic digestion system. *Water Science Technology*, *69*(2), 414–421.

Simon, D. (2006). *Optimal state estimation. Kalman, H_∞, and nonlinear approaches*. Wiley Interscience. USA.

Zeitz, M. (1984). Observability canonical (phase-variable) form for nonlinear time-variable systems. *International Journal of System Science*, *15*(9), 949–958.